0026-895X/09/7506-1380–1391$20.00
MOLECULAR PHARMACOLOGY
Vol. 75, No. 6
54395/3472926
Mol Pharmacol 75:1380–1391, 2009
Printed in U.S.A.

Evidence for Distinct Antagonist-Revealed Functional States of 5-Hydroxytryptamine$_{2A}$ Receptor Homodimers[S]

José Brea, Marián Castro, Jesús Giraldo, Juan F. López-Giménez, Juan Fernando Padín, Fátima Quintián, Maria Isabel Cadavid, Maria Teresa Vilaró, Guadalupe Mengod, Kelly A. Berg, William P. Clarke, Jean-Pierre Vilardaga, Graeme Milligan, and Maria Isabel Loza

Departamento de Farmacología, Instituto de Farmacia Industrial, Facultad de Farmacia, Universidad de Santiago de Compostela, Santiago de Compostela, Spain (J.B., M.C., J.F.P., F.Q., M.I.C., M.I.L.); Institut de Neurociències and Unitat de Bioestadística, Universitat Autònoma de Barcelona, Bellaterra, Spain (J.G.); Department of Biochemistry and Molecular Biology, University of Glasgow, Glasgow, United Kingdom (J.F.L.-G., G.M.); Department of Neurochemistry and Neuropharmacology, Instituto de Investigaciones Biomédicas de Barcelona, Consejo Superior de Investigaciones Cientificas, IDIBAPS, Barcelona, Spain (M.T.V., G.M.); Department of Pharmacology, University of Texas Health Science Center, San Antonio, Texas (W.P.C., K.A.B.); Department of Pharmacology and Chemical Biology, University of Pittsburgh Medical Center, Pittsburgh, Pennsylvania (J.-P.V.); and Endocrine Unit, Massachusetts General Hospital, and Harvard Medical School, Boston Massachusetts (J.-P.V.)

Received December 23, 2008; accepted March 11, 2009

ABSTRACT

The serotonin (5-hydroxytryptamine; 5-HT) 2A receptor is a cell surface class A G protein-coupled receptor that regulates a multitude of physiological functions of the body and is a target for antipsychotic drugs. Here we found by means of fluorescence resonance energy transfer and immunoprecipitation studies that the 5-HT$_{2A}$-receptor homodimerized in live cells, which we linked with its antagonist-dependent fingerprint in both binding and receptor signaling. Some antagonists, like the atypical antipsychotics clozapine and risperidone, differentiate themselves from others, like the typical antipsychotic haloperidol, antagonizing these 5-HT$_{2A}$ receptor-mediated functions in a pathway-specific manner, explained here by a new model of multiple active interconvertible conformations at dimeric receptors.

G protein-coupled receptors (GPCRs) constitute the major family of cell surface proteins involved in cell signaling cascades and are the target of ≈50% of clinical drugs (Imming et al., 2006). Studies on ligand-GPCR interactions performed over the last decade have revealed diverse capacities of ligand-GPCR-effector complexes to fine-tune their own signals, broadening its apparent simplicity and highlighting ligands as individual chemical species capable of transmitting messages into cellular function with a versatility unpredicted two decades ago (Kenakin, 2007b; Urban et al., 2007). It is well accepted that agonist (full and partial) ligands and allosteric-positive regulators can invoke different active conformations of GPCRs and that these may allow differential agonist-dependent regulation of signaling pathways. Such effects have been described as "agonist-directed trafficking of receptor stimulus" (Kenakin, 1995), "biased agonism" (Jarpe et al., 1998), "functional selectivity" (Urban et al., 2007), or "collateral efficacy" (Kenakin, 2007a). This recently accumulated experimental evidence has led to the development of novel mathematical representations that attempt to explain the chemical biology of GPCRs and integrate the new knowl-

This work was supported by the Ministerio de Educación y Ciencia, Spain [Grants SAF2007-65913, SAF2005-08025-C03]; the Xunta de Galicia [Grant PGIDIT06PXID203186PR, 2007/118]; and by Red Temática de Investigación Cooperativa COMBIOMED from Instituto de Salud Carlos III and Fundació La Marató de TV3 [Reference 070530].

J.B., M.C., and J.G. contributed equally to this work.

Article, publication date, and citation information can be found at http://molpharm.aspetjournals.org.
doi:10.1124/mol.108.054395.

[S] The online version of this article (available at http://molpharm.aspetjournals.org) contains supplemental material.

ABBREVIATIONS: GPCR, G protein-coupled receptor; 5-HT, 5-hydroxytryptamine, serotonin; AA, arachidonic acid; CHO, Chinese hamster ovary; (±)DOB, (±)-1-(4-bromo-2,5-dimethoxyphenil)-2-aminopropane; (±)DOI, (±)-1-(2,5-dimethoxy-4-iodophenyl)-2-aminopropane; FCS, fetal calf serum; GR55562, (3-[3-(dimethylamino)propyl]-4-hydroxy-*N*-[4-(4-pyridinyl)phenylbenzamide dihydrobromide]; IP, inositol phosphate; MDL100,907, (*R*)-(±)-4-[1-hydroxy-1(2,3-dimethoxyphenyl)metyhyl]*N*-2–4-fluorophenylethyl)piperidine; PLA$_2$, phospholipase A$_2$; PLC, phospholipase C; HEK, human embryonic kidney; MEM, minimum essential medium; PCR, polymerase chain reaction; CFP, cyan fluorescent protein; YFP, yellow fluorescent protein; FRET, fluorescence resonance energy transfer; RIPA, radioimmunoprecipitation assay; PAGE, polyacrylamide gel electrophoresis; TTBS, Tris-buffered saline/Tween 20; compound 40/80, *p*-methoxy-*N*-methyl-phenethylamine.

edge by extending accepted traditional models (De Lean et al., 1980; Kent et al., 1980; Lefkowitz et al., 1993; Samama et al., 1993; Leff, 1995; Weiss et al., 1996; Leff et al., 1997; Scaramellini and Leff, 2002).

Although it is generally believed that antagonists (neutral antagonists and inverse agonists) simply inhibit either agonist-induced or constitutive receptor functions, it is conceptually plausible to envision that certain antagonists could also deactivate GPCR responses in a ligand- and pathway-specific manner. A series of observations, including the ability of certain ligands that are conventionally described as "antagonists" to induce receptor internalization (Baker and Hill, 2007; Kenakin, 2007b), to cause activation of extracellular signal-regulated kinase mitogen-activated protein kinase (Azzi et al., 2003; Wisler et al., 2007), or to promote inverse agonist-specific receptor conformational changes (Vilardaga et al., 2005), are consistent with such a concept. This is particularly relevant because most current drugs that target GPCRs are antagonists.

In the last decade, there has been growing evidence to indicate that GPCR dimerization may be a requisite for function and that binding of small ligands to these receptors occurs on dimeric receptor forms (Ayoub et al., 2002; Milligan, 2004; Herrick-Davis et al., 2005), although monomeric forms of GPCRs have also been shown to be capable of activating G proteins (Bayburt et al., 2007; Whorton et al., 2007), suggesting that functionally active monomeric and dimeric forms of the receptors may coexist in equilibrium. Mechanisms by which ligands differentially regulate signaling pathways mediated by a single receptor generally considered the ability of ligands to differentially stabilize distinct receptor conformations (Hunton et al., 2005). The question is to what extent these different conformations occur at a single or paired receptor.

The 5-HT$_{2A}$ receptor is a class A GPCR whose antagonists have important applications in the treatment of disorders of the cardiovascular and central nervous systems (Berg et al., 2005), as well as in virology (Elphick et al., 2004). 5-HT$_{2A}$ receptors regulate IP accumulation mediated by phospholipase C and AA release mediated at least partially by phospholipase A$_2$, and different 5-HT$_{2A}$ receptor agonists, for instance serotonin and the hallucinogenic 2,5-dimethoxy-4-iodoamphetamine [(±)DOI], show functional selectivity discriminating between these two signaling pathways (Berg et al., 1998). In a previous study (López-Giménez et al., 2001), in native human brain and in cell lines expressing recombinant human 5-HT$_{2A}$ receptors lacking constitutive activity, we observed Gpp(NH)p-independent shallow, biphasic, competition binding curves for antagonists competing with agonist radioligands. In light of current knowledge (Wreggett and Wells, 1995; Chidiac et al., 1997; Armstrong and Strange, 2001; El-Asmar et al., 2005; Franco et al., 2005, 2006; Urizar et al., 2005), shallow and steep binding curves in studies using competitive ligands are consistent with receptor dimerization (Albizu et al., 2006), although it requires discarding other pharmacological features such as G-protein stoichiometry (Giraldo, 2008). However, 5-HT$_{2A}$ receptor dimerization has never been directly demonstrated, although it has been described for the 5-HT$_{2C}$ receptor, which shares high sequence homology with the 5-HT$_{2A}$ receptor (Herrick-Davis et al., 2004, 2005, 2006). The aim of the present study was to investigate 5-HT$_{2A}$ receptors dimerization and to gain insight into its functional relevance.

Materials and Methods

Cell Culture. CHO cells stably expressing human 5-HT$_{2A}$ receptors at ≈200 fmol/mg protein (CHO-FA4 cells) were maintained in Dulbecco's modified Eagle's medium-F12 supplemented with 10% (v/v) fetal calf serum (FCS), 1% L-glutamine, and 300 μg/ml hygromycin. HEK293 cells were maintained in minimum essential medium (MEM) Eagle supplemented with 10% (v/v) FCS, 1 mM MEM sodium pyruvate, 1% (v/v) MEM nonessential amino acid solution, 100 U/ml penicillin, and 0.1 mg/ml streptomycin. Cells were grown at 37°C in a 5% CO_2 humidified atmosphere.

Receptor Binding Studies at Human 5-HT$_{2A}$ Receptors. These assays were performed in membranes from CHO-FA4 cells following previously described protocols (López-Giménez et al., 2001). Under the experimental conditions established [5 nM [^{3}H](±)DOB as radioligand, 200–250 μg of protein per tube, and defining nonspecific binding with 10 μM mianserin], specific binding was approximately 75% of total binding.

Measurement of IP Accumulation and AA Release. For these experiments, cells were seeded into 12-well tissue culture plates at a density of 4×10^4 cells/cm^2. Measurement of IP accumulation and AA release were made simultaneously from the same well (Berg et al., 1998, 1999). In brief, cells were labeled with 1 μCi/ml [*myo*-^{3}H]inositol (20 Ci/mmol) for 24 h and with 0.1 μCi/ml [^{3}H]AA (200 Ci/mmol) for 4 h at 37°C. After the labeling period, cells were washed and then incubated in 1 ml of experimental medium (Hanks' balanced salt solution, 20 mM LiCl, and 20 mM HEPES) containing vehicle (H_2O) or the indicated concentrations of drugs at 37°C for 10 min. At the end of the incubation period, aliquots (200 μl) of media were added directly to scintillation vials for the measurement of ^{3}H content, which corresponds to AA release (Berg et al., 1998, 1999). The remaining medium was discarded, and 1 ml of 10 mM formic acid (4°C) was added to the wells to extract the accumulated [^{3}H]IP from the cells (IP_1, IP_2, and IP_3, collectively referred to as IP). The released [^{3}H]IP were separated by the anion exchange chromatography method of Berridge et al. (1982) and counted in a liquid scintillation counter (Beckman LS-6000 LL; Beckman Coulter, Fullerton, CA).

cDNA Constructs. The FLAG epitope was introduced at the N terminus of the human 5-HT$_{2A}$ receptor by PCR with a forward primer containing the sequence of the FLAG epitope (amino acid sequence DYKDDDDK). The c-myc epitope was introduced at the N terminus of the human 5-HT$_{2A}$ receptor by PCR with a forward primer containing the sequence of the c-myc epitope (amino acid sequence EQKLISEEDL). Fusion proteins of c-myc-5-HT$_{2A}$ receptor with cyan fluorescent protein (CFP) or enhanced yellow fluorescent protein (YFP) (5-HT$_{2A}$R^{CFP} and 5-HT$_{2A}$R^{YFP}, respectively) were constructed by ligation of two PCR products corresponding to the receptor sequence without stop codon and to each fluorescent protein sequence, amplified from their original plasmids (Clontech, Mountain View, CA), introducing a NotI endonuclease restriction site. The ligation products were subcloned into pcDNA3 plasmid (Invitrogen, Carlsbad, CA) and verified by DNA sequencing.

Transient Transfection of HEK293 Cells for Coimmunoprecipitation and FRET Experiments. For coimmunoprecipitation experiments, HEK293 cells seeded on 100-mm dishes were transiently transfected with 10 μg/dish of total DNA following the calcium phosphate method (Cullen, 1987). For FRET photobleaching experiments, HEK293 cells were grown on poly(D-lysine)-treated glass coverslips in 60-mm dishes to approximately 60 to 80% confluence before transient transfection with the different CFP/enhanced YFP fusion proteins using Effectene transfection reagent (Qiagen GmbH, Hilden, Germany), according to the manufacturer's instructions. The total amount of DNA in the different transfections was held constant with plasmid pcDNA3. Both in coimmunoprecipitation

and FRET experiments, FCS was substituted by dialyzed FCS in the corresponding growing media for maintenance of the transiently transfected cells until the time of the experiment (36 h after transfection).

Coimmunoprecipitation Studies. Coimmunoprecipitation studies using FLAG- and c-myc-tagged forms of the 5-HT_{2A} receptor were performed in transiently transfected HEK293 cells. The different coimmunoprecipitation samples corresponded to the following cDNA combinations and transfection conditions: "mock" (10 μg/dish of vector pcDNA3); "FLAG" (10 μg/dish of FLAG-5-HT_{2A} construct); "myc" (10 μg/dish of c-myc-5-HT_{2A} construct); and "FLAG + myc" (5 μg of FLAG-5-HT_{2A} construct + 5 μg/dish of c-myc-5-HT_{2A} construct/dish). Cells were harvested 36 h after transfection in 10 ml/dish of ice-cold phosphate-buffered saline, and the "mix" sample was prepared at this point by 1:1 mixing of 5 ml of a harvested additional "FLAG"-transfected dish and 5 ml of a harvested additional "myc"-transfected dish. Cells were pelleted by centrifugation at 300*g* for 10 min, and the pellets were homogenized in 1 ml of 1× RIPA buffer (50 mM HEPES, 150 mM NaCl, 1% Triton X-100, 0.5% sodium deoxycholate, and 0.1% SDS) supplemented with 10 mM NaF, 5 mM EDTA, 10 mM NaH_2PO_4, 5% ethylene glycol, and a protease inhibitor cocktail (Protease Inhibitor Cocktail for general use; Sigma, St. Louis, MO), pH 7.3, and placed on a rotating wheel at 4°C for 1 h. The samples were then centrifuged for 10 min at 14,000*g* at 4°C, and the supernatants were precleared by incubating them with 50 μl of protein G (Protein G-Sepharose 4B fast flow; Sigma-Aldrich, St. Louis, MO) at 4°C on a rotating wheel for 1 h. After this, the samples were centrifuged at 14,000*g* at 4°C for 1 min, the cleared supernatant was transferred to a fresh tube, and the protein concentration in the supernatants was determined with a bicinchoninic acid assay protein quantification kit (Uptima, Interchim, France). The protein concentration of individual samples was adjusted to 0.8 mg/ml using 1× RIPA, and 600 μl of each sample was incubated overnight with 40 μl of protein G and 5 μg of anti-FLAG M2 monoclonal antibody (Sigma) at 4°C on a rotating wheel after reserving a 100-μl sample of the supernatants for the assessment of protein expression in the cell lysates. Sixteen hours later, the rotating samples were centrifuged at 14,000*g* for 1 min at 4°C, and the protein G beads were washed three times with 1 ml of 1× RIPA buffer and resuspended in 40 μl of 2× reducing Laemmli buffer. Reducing Laemmli buffer (6×) was also added to the lysates, and both immunoprecipitated samples and cell lysates were incubated at 37°C for 30 min and resolved by SDS-PAGE in 4 to 15% Tris-HCl polyacrylamide precast gels (Ready Gel precast gels; Bio-Rad, Hercules, CA). After electrophoresis, proteins were transferred to polyvinylidene difluoride membranes (Immun-Blot polyvinylidene difluoride membranes; Bio-Rad), which were blocked for 1 h in TTBS (10 mM Tris-HCl, pH 7.7, 0.9% NaCl, and 0.1% Tween 20) buffer containing 5% dehydrated nonfat milk. Subsequently, membranes were incubated overnight at 4°C with myc-tag rabbit polyclonal antibody (Cell Signaling Technology, Danvers, MA) diluted 1:11,000 in TTBS buffer containing 1% bovine serum albumin and 0.05% sodium azide (immunoprecipitated samples and cell lysates) or with 0.4 μg/ml anti-FLAG M2 monoclonal antibody (Sigma) in TTBS buffer containing 1% bovine serum albumin and 0.05% sodium azide (cell lysates). Goat anti-rabbit (1:5000 in TTBS) or sheep anti-mouse (1:10,000 in TTBS) peroxidase-conjugated secondary antibodies (GE Healthcare, Chalfont St. Giles, Buckinghamshire, UK) were used for detection by enhanced chemiluminescence using ECL Plus Western blotting chemiluminescence detection kit (GE Healthcare) and Hyperfilm ECL films (GE Healthcare).

Microscopic FRET Photobleaching Experiments. FRET between CFP and YFP in HEK293 cells transiently transfected with the different CFP/enhanced YFP constructs was determined in live cells by donor recovery after acceptor photobleaching following previously described protocols (Vilardaga et al., 2003). In brief, HEK293 cells grown on coverslips were maintained in HEPES buffer (137 mM NaCl, 5 mM KCl, 1 mM $CaCl_2$, 1 mM $MgCl_2$, and 20 mM HEPES, pH 7.4) at room temperature (22°C) and placed on an Eclipse TE2000-U fluorescence inverted microscope (Nikon) equipped with an oil immersion 100× objective and a dual emission photometric system (TILL Photonics, Gräfelfing, Germany). Samples were excited with a xenon lamp from a polychrome V (TILL Photonics). The emission fluorescence intensities of the fluorescent constructs were determined at 535 ± 15 nm (YFP) and 480 ± 15 nm (CFP) with a beam splitter dichroic long-pass of 505 nm, upon excitation at 436 nm (filter 436 ± 10 nm and a beam splitter dichroic long-pass of 455 nm), resulting the bleed-through of YFP into the 480-nm channel negligible. The emission intensities of CFP were recorded before (CFP_{before}) and after (CFP_{after}) 1 min of direct illumination of YFP at 500 nm. FRET efficiency was calculated according to eq. 1:

$$\text{FRET efficiency (\%)} = \frac{CFP_{after} - CFP_{before}}{CFP_{before}} \times 100 \qquad (1)$$

To ensure that the groups of cells analyzed in the different experiments were similar in terms of their fluorescence characteristics, the levels of YFP expression were determined at the beginning of each experiment as the emission intensity of YFP (recorded at 535 nm) upon direct excitation at 500 nm and the levels of expression of CFP in each cell were determined as the emission intensity of CFP after photobleaching. Fluorescence emission signals detected by avalanche photodiodes were digitalized using an analog-to-digital converter (Digidata1322A; Molecular Devices, Sunnyvale, CA) and stored on personal computer using Clampex 9.0 (Molecular Devices). Data were analyzed using the programs Origin (OriginLab Corp, Northampton, MA) and Prism 4.0 (GraphPad Software Inc., San Diego CA).

Drugs. [^{3}H](±)DOB (23.1 Ci/mmol) was purchased from PerkinElmer Life and Analytical Sciences (Waltham, MA). [*myo*-^{3}H]Inositol (20 Ci/mmol) and [^{3}H]arachidonic acid (200 Ci/mmol) were supplied by American Radiolabeled Chemical (St. Louis, MO). Ketanserin, mesulergine, clozapine, and all other drugs and chemicals were reagent-grade products from Sigma/RBI (Alcobendas, Spain). MDL100,907 was a generous gift from Dr. M. Galvan (Marion Merrell Dow, Strasbourg, France).

Data Analysis and Mathematical Modeling. Binding and stimulation response data were fitted by the Hill eq. 2 with Prism software:

$$y = \text{Bottom} + \frac{\text{Top} - \text{Bottom}}{1 + 10^{n_H(\log EC_{50} - x)}} \qquad (2)$$

where y is the response variable, x is the log[A]; [A] is the ligand concentration; Top and Bottom are the maximum and minimum responses, respectively; EC_{50} is the ligand concentration for half-maximum response; and n_H is the Hill coefficient. Discrimination between one site and two noninterconverting sites for antagonist binding competition curves was performed by comparing the fit provided by eqs. 3 and 4:

$$y = \frac{100}{1 + 10^{x - \log IC_{50}}} \qquad (3)$$

$$y = 100\left(\frac{f}{1 + 10^{x - \log IC_{50_1}}} + \frac{1 - f}{1 + 10^{x - \log IC_{50_2}}}\right) \qquad (4)$$

where x is the log[B] and B is the antagonist, IC_{50} is the concentration of antagonist that inhibits 50% of the specific radioligand binding for a single binding site receptor, and agonist binding in the absence of antagonist is 100%. In the case of two binding sites (eq. 4), IC_{50_1} and IC_{50_2} are the IC_{50} values for sites 1 and 2, respectively, and f and (1-f) the corresponding fractions of receptor sites.

Curve-Fitting by the Three-State Dimer Receptor Model: Binding and Function. The receptor model shown in Fig. 5 was used for curve-fitting. For the binding of an agonist A in the presence of a varying concentration of an antagonist B, eq. 12 leads to eq. 5,

where the constants c_1 to c_5 are combinations of the mechanistic constants included in the model.

$$y = \frac{[A]_{Bound}}{2[R_T]} = \frac{1}{2}\left(\frac{c_1[A] + 2[A]^2 + c_5[A][B]}{c_2 + c_1[A] + [A]^2 + (c_3 + c_5[A])[B] + c_4[B]^2}\right) \quad (5)$$

Equation 5 can be rearranged into eq. 6 (percentages) by making $y = 100$ for a fixed concentration of ligand A.

$$y = 100\,\frac{a + b[B]}{a + c[B] + [B]^2} \quad (6)$$

It can be shown that eqs. 4 and 6 are the same by making $a = IC_{50_1}IC_{50_2}$, $b = f \cdot IC_{50_1} + (1 - f)IC_{50_2}$, and $c = IC_{50_1} + IC_{50_2}$. Thus, from a statistical point of view, to state that a two-noninterconvertible sites model fits data better than a one-site model is equivalent to saying that a dimer receptor model fits data better than a one-site receptor model.

The equation for the functional response for either [^{3}H]IP accumulation or [^{3}H]AA release pathway is given by eq. 7 (an empirical relationship resulting from the mechanistic eqs. 13 and 14), where c_1 to c_5 are combinations of the equilibrium constants included in the model (Fig. 5).

$$y = \frac{c_1 + c_2[A] + c_3[A]^2}{c_4 + c_5[A] + [A]^2} \quad (7)$$

In the same way as in the binding studies (see above), the percentage of functional response of a fixed concentration of an agonist A in the presence of varying concentrations of a ligand B is given by eq. 8, where a value of 100 is assigned to the activity of the agonist A in the absence of B.

$$y = 100\,\frac{a + b[B] + c[B]^2}{a + d[B] + [B]^2} \quad (8)$$

To assess whether biphasic curves are present, the goodness of fit for eq. 8 was compared with that for the monophasic eq. 9.

$$y = 100\,\frac{1}{1 + \frac{[B]}{IC_{50}}} \quad (9)$$

Statistical Comparisons between Models: The *F* Test. Statistical comparisons between fits provided by eqs. 3 and 4 or between eqs. 8 and 9 were performed by the extra sum-of-squares *F* test (Giraldo et al., 2002). The *F* statistic, which allows for the comparison between models if they are nested (one model can be formulated as a particular case of the other), is constructed as

$$F = \frac{\frac{SS_1 - SS_2}{df_1 - df_2}}{\frac{SS_2}{df_2}} \quad (10)$$

where SS is the residual sum of squares, *df* is the degrees of freedom, and the subscripts 1 and 2 correspond to the model with fewer and greater number of parameters, respectively. Statistical significance was set at $P < 0.05$.

Assessing Affinity Constants for the Antagonists. K_i values were calculated with the Cheng-Prusoff equation (Cheng and Prusoff, 1973). Calculation of pA_2 values for clozapine was performed as described by Arunlakshana and Schild (1959). After incubation of the antagonist, calculation of the apparent antagonist dissociation constant (K_B) was determined by linear regression with eq. 11:

$$\log(dr - 1) = \log[B] - \log K_B \quad (11)$$

where [B] is the concentration of the antagonist used and *dr* represents the ratio (dose ratio) of concentrations of the agonist (EC_{50}) that produce identical responses (50% E_{max}) in the presence and absence of the antagonist. A Schild analysis was performed with three different concentrations of the antagonist, and then the antagonistic potency of clozapine was expressed as pA_2 (the value of [B] for $\log(dr - 1) = 0$) and given as mean ± S.E.M. Affinity constants obtained by Cheng-Prusoff and Schild analyses are considered as exploratory rather than as accurate parameter values. This is because these methods were originally developed for the simplest (A + R = AR) ligand-receptor interaction model. Given the increasing complexity of GPCR models, constant estimates by Schild and Cheng-Prusoff methods should be treated with caution. As recently shown (Giraldo et al., 2007), inclusion of inverse agonism affects the intercept of eq. 11 but not the slope, which remains equal to 1. A slope in eq. 11 different from 1 is expected in receptor dimer models if cooperativity occurs.

Results

5-HT$_{2A}$ Receptors Form Homo-Oligomers in Live Cells. The presence of 5-HT$_{2A}$ receptor homo-complexes in transfected cell lines was investigated by two sets of experiments. First, coexpression of N-terminally c-myc- or FLAG-tagged 5-HT$_{2A}$ receptors in HEK293 cells followed by immunoprecipitation of the cell lysates with anti-FLAG antibodies and immunoblotting with anti-c-myc antibodies revealed the coimmunoprecipitation of a major immunoreactive band of approximately 55 kDa, corresponding to a c-myc-tagged protein of molecular weight similar to that described for the 5-HT$_{2A}$ receptor (Wu et al., 1998) (Fig. 1a, top, "FLAG + myc" line). The anti-c-myc immunoreactivity was not detected when the c-myc- and FLAG-tagged receptors were not expressed in the same cells (Fig. 1a, top, "mix" line), nor when singly expressed FLAG- and myc-receptors were mixed together before immunoprecipitation (Fig. 1a, top, "FLAG" and "myc" lines), ruling out the formation of oligomers or receptor aggregates during the solubilization process and denaturation of the samples before SDS-PAGE. The expression of the differently tagged receptors in these experiments was verified in the cell lysates by immunoblotting with anti-FLAG and anti-c-myc antibodies (Fig. 1a, middle and bottom).

Second, we measured FRET efficiency between 5-HT$_{2A}$ receptors C-terminally tagged with CFP and YFP (5-HT$_{2A}$R^{CFP} and 5-HT$_{2A}$R^{YFP}, respectively) coexpressed in HEK293 cells by measuring donor recovery after acceptor photobleaching (Fig. 1b). The experiments yielded a FRET efficiency between the two fluorescent 5-HT$_{2A}$ receptors of 5.97 ± 0.794% (mean ± S.E.M., $n = 22$) (Fig. 1c). This value was significantly higher ($P < 0.001$) than the FRET efficiency measured in HEK293 cells showing similar CFP and YFP fluorescent levels but coexpressing a control pair of proteins consisting of 5-HT$_{2A}$R^{CFP} and N-terminally membrane-tagged YFP (YFP^m) for the assessment of nonspecific FRET as a result of random distribution and collision between fluorescent proteins (FRET efficiency = 1.01 ± 0.322%, mean ± S.E.M., $n = 15$) (Fig. 1c). FRET efficiencies between 5-HT$_{2A}$R^{YFP} coexpressed with other C-terminally CFP-tagged GPCRs, for which interaction with 5-HT$_{2A}$ receptors is not reported such as the dopamine-1A receptor and the parathyroid hormone receptor type 1 ($D_{1A}R^{CFP}$ and PTHR^{CFP}, respectively) were (mean ± S.E.M.) 1.92 ± 0.407% and 2.11 ± 0.354%, $n = 12$ and 15, for $D_{1A}R^{CFP}$ + 5-HT$_{2A}$R^{YFP} and PTHR^{CFP} + 5-HT$_{2A}$R^{YFP}, respectively, not significantly different from the nonspecific FRET detected between 5-HT$_{2A}$R^{CFP} and YFP^m among groups of cells dis-

playing similar fluorescence levels (Fig. 1c). Further analysis of the results revealed that the FRET efficiency between 5-$HT_{2A}R^{CFP}$ and 5-$HT_{2A}R^{YFP}$ increased as a hyperbolic function of the level of acceptor expression and reached a maximal value when most of the donor molecules would be complexed with acceptor molecules (Fig. 1d), a behavior expected for specific protein/protein oligomerization (Mercier et al., 2002; Zacharias et al., 2002). Conversely, FRET efficiency between 5-$HT_{2A}R^{CFP}$ and YFP^m increased linearly with the acceptor expression level, as typically expected from random interactions between fluorescent proteins.

Antagonists Differentiate Distinct 5-HT_{2A} Receptor Signaling Conformations. We compared the capacity of two well known antipsychotic antagonists, clozapine and haloperidol, to compete with the agonist [^{3}H](±)DOB. The atypical antipsychotic clozapine displayed Gpp(NH)p-independent biphasic competition binding curves for (±)DOB-bound 5-HT_{2A} receptors, whereas the typical antipsychotic haloperidol displayed a monophasic competition binding profile (Fig. 2a). Similar mono- or biphasic profiles also differentiated another series of antagonists, which indicate a selective antagonist-dependent curve shape at the 5-HT_{2A} receptor (Table 1 and Supplementary Fig. 1a).

We then assessed the signaling properties of the 5-HT_{2A} receptor by simultaneously measuring the formation of IP and the release of AA after agonist stimulation following a

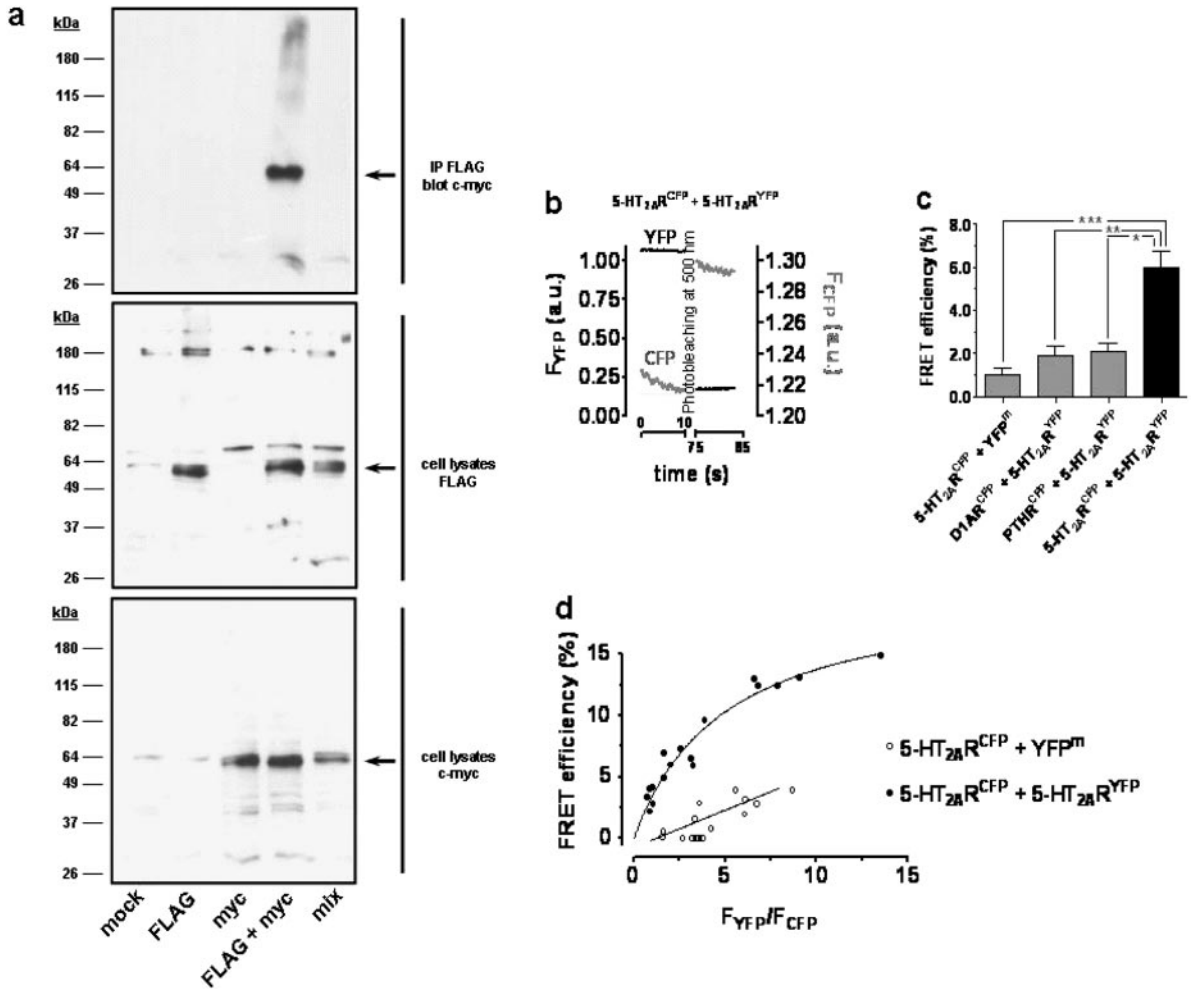

Fig. 1. Analysis of the association of 5-HT_{2A} receptors in transfected cells. a, coimmunoprecipitation of differentially epitope-tagged forms of the human 5-HT_{2A} receptor: evidence for constitutive homo-oligomerization. Top, HEK293 cells were transiently transfected with empty vector ("mock" line), the cDNA encoding the FLAG-5-HT_{2A} receptor ("FLAG" line), the cDNA encoding the c-myc-5-HT_{2A} receptor ("myc" line), or cDNAs for both the FLAG-5-HT_{2A} and c-myc-5-HT_{2A} receptors ("FLAG + myc" line). Before immunoprecipitation, cell lysates from cells separately expressing FLAG-5-HT_{2A} and c-myc-5-HT_{2A} receptors were physically mixed ("mix" line). Cell lysates were immunoprecipitated with anti-FLAG antibodies, the samples resolved by SDS-PAGE, and then immunoblotted with anti-c-myc. Middle and bottom, expression of FLAG-5-HT_{2A} and c-myc-5-HT_{2A} receptors in the differently transfected HEK293 cells was verified in the cell lysates by immunoblotting with anti-FLAG and anti-c-myc antibodies. b, a typical photobleaching experiment. Emission intensities of YFP (535 nm, black) and CFP (480 nm, gray) recorded from single cells coexpressing 5-$HT_{2A}R^{CFP}$ and 5-$HT_{2A}R^{YFP}$ receptors using fluorescence microscopy. Emission intensities were recorded before and after YFP was photobleached by 1-min exposure to continue illumination at 500 nm. c, FRET efficiency calculated as described under *Materials and Methods* from cells expressing different pairs of CFP- or YFP-tagged proteins. ***, $P < 0.001$; **, $P < 0.01$; and *, $P < 0.05$, for 5-$HT_{2A}R^{CFP}$ + 5-$HT_{2A}R^{YFP}$ versus 5-$HT_{2A}R^{CFP}$ + YFP^m, D1AR^{CFP} + 5-$HT_{2A}R^{YFP}$, and $PTHR^{CFP}$ + 5-$HT_{2A}R^{YFP}$, respectively, one-way analysis of variance and Dunn's multiple comparison test. Average CFP intensities for the different pairs were (mean ± S.E.M., a.u.) 1.33 ± 0.156 (n = 15), 1.25 ± 0.125 (n = 12), 1.25 ± 0.150 (n = 15), and 1.30 ± 0.161 (n = 22), and donor/acceptor ratios were (mean ± S.E.M.) 3.18 ± 0.374, 2.85 ± 0.484, 2.82 ± 0.370, and 2.89 ± 0.359 for 5-$HT_{2A}R^{CFP}$ + YFP^m, D1AR^{CFP} + 5-$HT_{2A}R^{YFP}$, $PTHR^{CFP}$ + 5-$HT_{2A}R^{YFP}$, and 5-$HT_{2A}R^{CFP}$ + 5-$HT_{2A}R^{YFP}$, respectively. d, values of FRET efficiency from cells coexpressing 5-$HT_{2A}R^{CFP}$ + 5-$HT_{2A}R^{YFP}$ or 5-$HT_{2A}R^{CFP}$ + YFP^m. Data for 5-$HT_{2A}R^{CFP}$ + YFP^m were directly proportional to the acceptor/donor ratio, whereas FRET efficiency values for 5-$HT_{2A}R^{CFP}$ + 5-$HT_{2A}R^{YFP}$ followed a hyperbolic function of acceptor/donor ratio.

previously described protocol (Berg et al., 1998, 1999). Application of serotonin to CHO-FA4 cells stably expressing the 5-HT$_{2A}$ receptor stimulated IP formation and AA release in a concentration-dependent manner. Half-maximal activation occurred at a concentration similar to that of serotonin at the two pathways (pEC$_{50}$ = 6.56 ± 0.37 and 6.60 ± 0.25 for IP formation and AA release, respectively), and with identical Hill coefficients ≈1 (n_H = 0.99 ± 0.06 and 1.08 ± 0.11 for IP formation and AA release, respectively) (Fig. 3a).

Second, we compared the ability of diverse antagonists to block 5-HT$_{2A}$ receptor signals. Clozapine inhibited serotonin-induced IP accumulation with a monophasic profile and an IC$_{50}$ value of 89.12 ± 3.10 nM. Conversely, this compound showed an inhibition profile of AA release better described by a biphasic curve (F test, $P < 0.01$) that yield IC$_{50}$ values of 2.04 ± 0.51 and 4176 ± 1458 nM for each of the phases and with 56.33% of the sites corresponding to the high-affinity fraction of receptors (Fig. 2b). Increasing concentrations of clozapine induced parallel rightward shifts of the serotonin-stimulated IP response (pA$_2$ for clozapine-antagonism of 5-HT-induced IP accumulation = 7.98 ± 0.16), and Schild regression analysis of these shifts yielded a slope ≈1 (0.948 ± 0.160) (Fig. 3b). These data correspond well with the predicted property of a competitive antagonist. However, when serotonin-induced AA release was analyzed by Schild analysis, the shifts in the 5-HT concentration-response curves were surmountable, but not parallel, with a slope of 0.34 ± 0.19, indicative of noncompetitive or allosteric antagonism (Fig. 3c). Similar inhibitory effects of clozapine were observed when the 5-HT$_{2A}$ receptor was activated by another selective agonist, (±)DOI (Supplementary Fig. 2, a and b).

The monophasic versus biphasic inhibitory profiles of clozapine at the serotonin-mediated IP and AA pathways were preserved after inhibition of PLA$_2$ or PLC, respectively, with selective inhibitors in the cells. Hence, pretreatment of the cells with the PLC inhibitor compound 48/80 (100 μM), which inhibited by 40% the serotonin-induced [^{3}H]IP accumulation, did not alter the biphasic inhibition profile of clozapine at the AA pathway (Fig. 4, a and b, and Supplementary Table 1). In the same way, the monophasic inhibition of IP accumulation by clozapine was not affected by pretreatment of the cells with a PLA$_2$ inhibitor (10 μM aristolochic acid), which inhibited by 85% the serotonin-induced [^{3}H]AA release (Fig. 4, a and c, and Supplementary Table 1). This eliminates cross-talk between IP and AA pathways as a cause of the clozapine pathway-dependent inhibition profile. Again, similar inhibition patterns for AA release and IP formation were observed for clozapine in the absence or presence of GR55562, a selective antagonist of the 5-HT$_{1B}$ receptor, discarding a potential contribution of this endogenous receptor subtype to the bi-

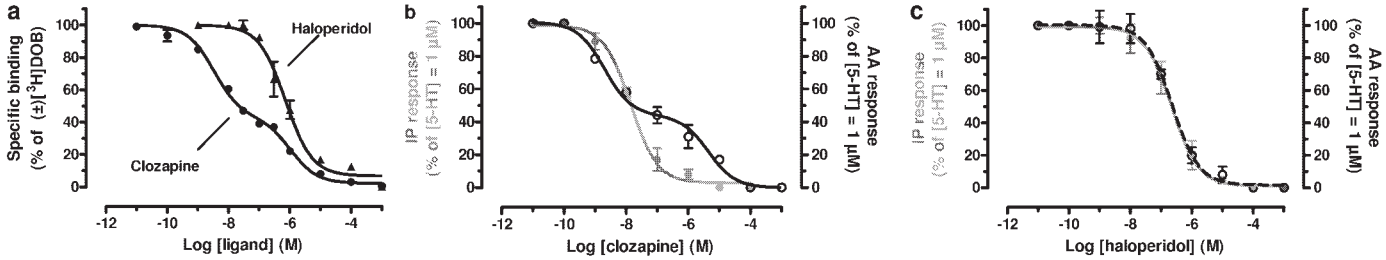

Fig. 2. Differential conformational recognition by clozapine and haloperidol at 5-HT$_{2A}$ receptors. a, [^{3}H](±)DOB binding displacement curves for clozapine and haloperidol at human 5-HT$_{2A}$ receptors stably transfected in CHO cells. Clozapine data were best-fitted to a two-site than to a one-site equation (F test, $P < 0.001$), whereas haloperidol data were best-fitted to a one-site equation (F test, $P > 0.05$). K_i values were 3.47 ± 0.50 and 1819 ± 166 nM for clozapine (high- and low-affinity sites, respectively) and 416.8 ± 59.4 nM for haloperidol. Error bars show S.E.M., and n = 3. b, inhibition curves for clozapine on 1 μM 5-HT-induced IP formation (filled gray circles) and AA release (open circles). Data for AA release were best-fitted to a two-site equation (F test, $P < 0.001$, n = 3), whereas IP formation data were best-fitted to a one-site equation (F test, $P > 0.05$, n = 3). Note that IC$_{50}$ values for AA release (2.04 ± 0.51 nM for the high- and 4176 ± 1458 nM for the low-affinity phase) are close to K_i values observed in binding competition studies. The IC$_{50}$ value for IP formation was 89.12 ± 3.10 nM. Error bars show S.E.M., n = 3. c, inhibition curves for haloperidol on 1 μM 5-HT-induced IP formation (filled gray circles) and AA release (open circles). Both AA and IP data were best-fitted to a one-site equation (F test, $P > 0.05$, n = 3). Note that IC$_{50}$ values for both effector pathways (223.8 ± 26.2 nM for IP formation and 234.4 ± 33.1 nM for AA release) were close to the K_i values observed in binding competition studies. Error bars show S.E.M.; n = 3.

TABLE 1

Competition parameters of several antagonists for [^{3}H](±)DOB-labeled receptors (binding assays) and for inhibition of 1 μM 5-HT-induced [^{3}H]IP accumulation and [^{3}H]AA release (functional assays) in CHO-FA4 cells expressing human 5-HT$_{2A}$ receptors

Values represent mean ± S.E.M. of at least three independent experiments performed in triplicate.

	Binding Assays			Functional Assays			
	K_i		High	[^{3}H]IP IC$_{50}$	[^{3}H]AA IC$_{50}$		High
	High	Low			High	Low	
	nM		%	*nM*	*nM*		%
Clozapine	3.47 ± 0.50	1819 ± 166	64.9	89.12 ± 3.10	2.04 ± 0.51	4176 ± 1458	56.33
Ketanserin[a]	4.36 ± 0.82	10964 ± 1021	24.1	9.77 ± 1.01	1.73 ± 0.60	7658 ± 139	29.74
Risperidone	0.16 ± 0.03	549.5 ± 195	60.4	0.89 ± 0.51	0.11 ± 0.03	309.1 ± 147.5	53.80
MDL100,907[a]	0.16 ± 0.02	380.2 ± 148	59.5	0.13 ± 0.02	0.07 ± 0.05	76.8 ± 18.2	49.95
Haloperidol		416.8 ± 59.4		223.8 ± 26.2		234.4 ± 33.1	
Mesulergine[a]		151.3 ± 9.95		199 ± 82		524.8 ± 124.0	

[a] Binding data are from López-Giménez et al. (2001).

phasic antagonist behavior (Fig. 4, a and d, and Supplementary Table 1).

The addition of serotonin to cells pretreated with clozapine for at least 15 min elicited the same profiles of inhibition as when the antagonist was added simultaneously with serotonin, eliminating different binding kinetics of agonists and antagonists as the mechanism responsible for the biphasic curves (Supplementary Fig. 3). These data support that clozapine antagonizes the IP pathway through a competitive mechanism, whereas the mechanism by which clozapine inhibits 5-HT_{2A} receptor-mediated AA responses would be determined by factors more complex than a simple ligand-receptor interaction.

As in the case of the binding assays, we found that additional antagonists also displayed the ability to inhibit 1 μM 5-HT-activated receptor responses by distinct mechanisms. Like clozapine, ketanserin, risperidone, and MDL100,907 each inhibited 5-HT-stimulated IP accumulation in a monophasic manner but showed biphasic inhibition of AA release (F test, $P < 0.05$) (Table 1 and Supplementary Fig. 1, b and c). In contrast, haloperidol and mesulergine inhibited 1 μM 5-HT-induced stimulation of both IP accumulation and AA release in a monophasic manner (Fig. 2c, Table 1, and Supplementary Fig. 1, b and c). Again for all of the antagonists, there was a strong correspondence between the negative cooperative binding parameters and the biphasic functional inhibition data obtained at the AA pathway (Table 1). These results therefore provide evidence of a functional antagonist-dependent negative cooperativity in the inhibition of the AA pathway that mirrors the antagonist-dependent negative cooperative binding indicative of 5-HT_{2A} receptor homodimers.

The Three-State Receptor Dimer Model. Our experimental data are consistent with a dimeric receptor with two active states, one for each biochemical pathway. We propose a model that is based on the existence of the receptor in equilibrium between its inactive dimeric form (R_2) and two distinct active [$(R_2)^*$ and $(R_2)^{**}$] receptor states (Fig. 5). The model, which can be considered an extension of both the recently described two-state dimer model (Franco et al., 2005, 2006) (by including an additional active receptor conformation), or the three-state monomer model (Leff et al., 1997) (by assuming that the receptor species are dimers instead of monomers), allows for the differential functional antagonist profiles by assuming a different receptor active conformation for each pathway [e.g., $(R_2)^*$ for IP accumulation and $(R_2)^{**}$ for AA release].

We aimed to use the model to account for the selectivity of curve shapes both for binding and response curves shown for some antagonists. Ligand-binding and ligand-response equations can be derived from the proposed model by including the proper receptor species.

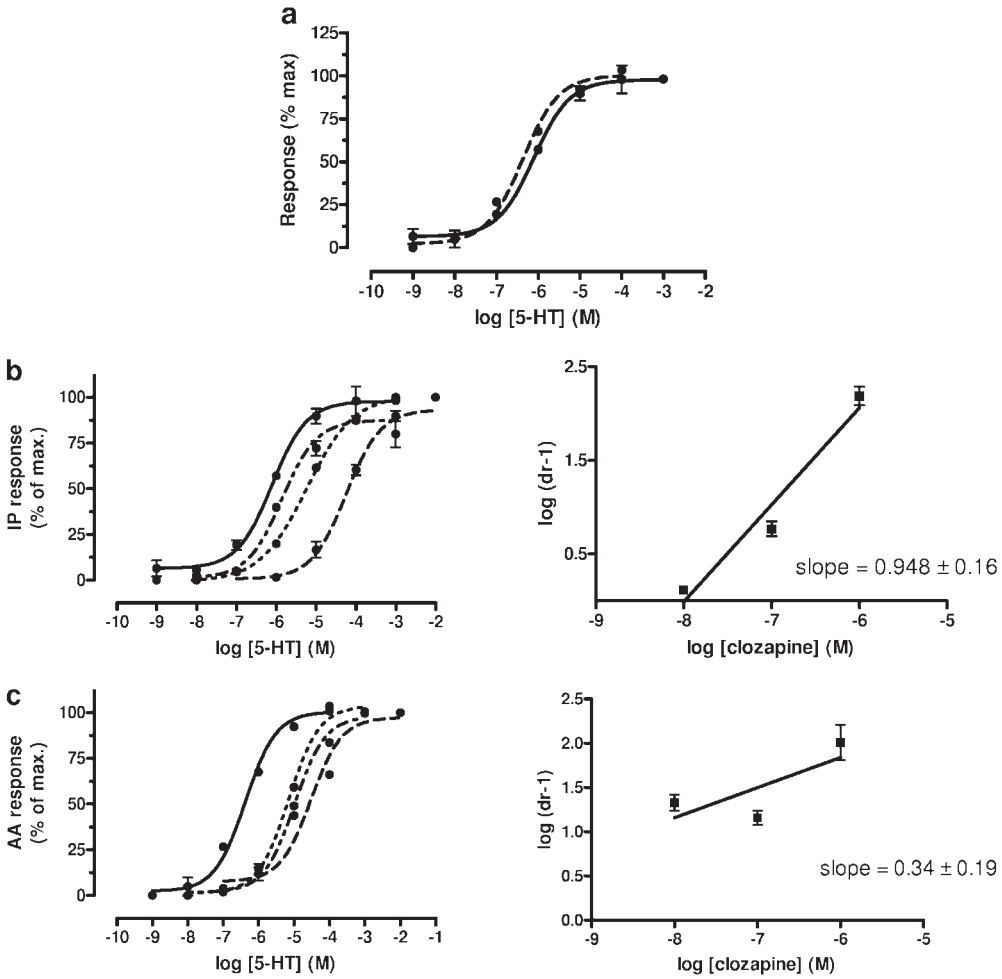

Fig. 3. Noncompetitive antagonism of clozapine at AA release pathway at 5-HT_{2A} receptors. a, concentration-response curves for 5-HT at IP formation (solid line) and AA release (broken line). b and c, concentration-response curves for 5-HT in the absence (solid line) and presence of 0.01 (– - - - - -), 0.1 (- - -), and 1 (– – –) μM clozapine at IP formation (b, left plot) and AA release (c, left plot). Schild plots slopes evidence a competitive antagonism for IP formation (b, right plot) but a noncompetitive antagonism for AA release (c, right plot). Error bars show S.E.M., $n = 3$.

Thus, the fractional binding of the agonist A in the presence of the antagonist B is defined as

$$y = \frac{[A_{bound}]}{2[R_t]}$$

$$= \frac{[A(R_2)] + 2[A_2(R_2)] + [A(R_2)^*] + 2[A_2(R_2)^*] + [A(R_2)^{**}] + 2[A_2(R_2)^{**}] + [AB(R_2)] + [AB(R_2)^*] + [AB(R_2)^{**}]}{2[R_t]} \quad (12)$$

The fractional response of the IP pathway is defined as

$$y_{R^*} = \frac{[(R_2)^*] + [A(R_2)^*] + [A_2(R_2)^*] + [B(R_2)^*] + [B_2(R_2)^*] + [AB(R_2)^*]}{2[R_t]} \quad (13)$$

The fractional response of the AA pathway is defined as

$$y_{R^{**}} = \frac{[(R_2)^{**}] + [A(R_2)^{**}] + [A_2(R_2)^{**}] + [B(R_2)^{**}] + [B_2(R_2)^{**}] + [AB(R_2)^{**}]}{2[R_t]} \quad (14)$$

Inclusion in these expressions of the mechanistic constants of the model (Fig. 5) and algebraic handling of the resulting equations leads to simplified empirical equations appropriate for curve-fitting (see *Materials and Methods*). This first description of such antagonist behavior in oligomeric receptors establishes a new theoretical model for the homodimeric arrangement of GPCRs, including an inactive (R_2) and two active [$(R_2)^*$ and $(R_2)^{**}$] receptor conformations. If we assign the $(R_2)^*$ to the IP accumulation and $(R_2)^{**}$ to AA release, our data indicate that an apparent negative cooperativity be-

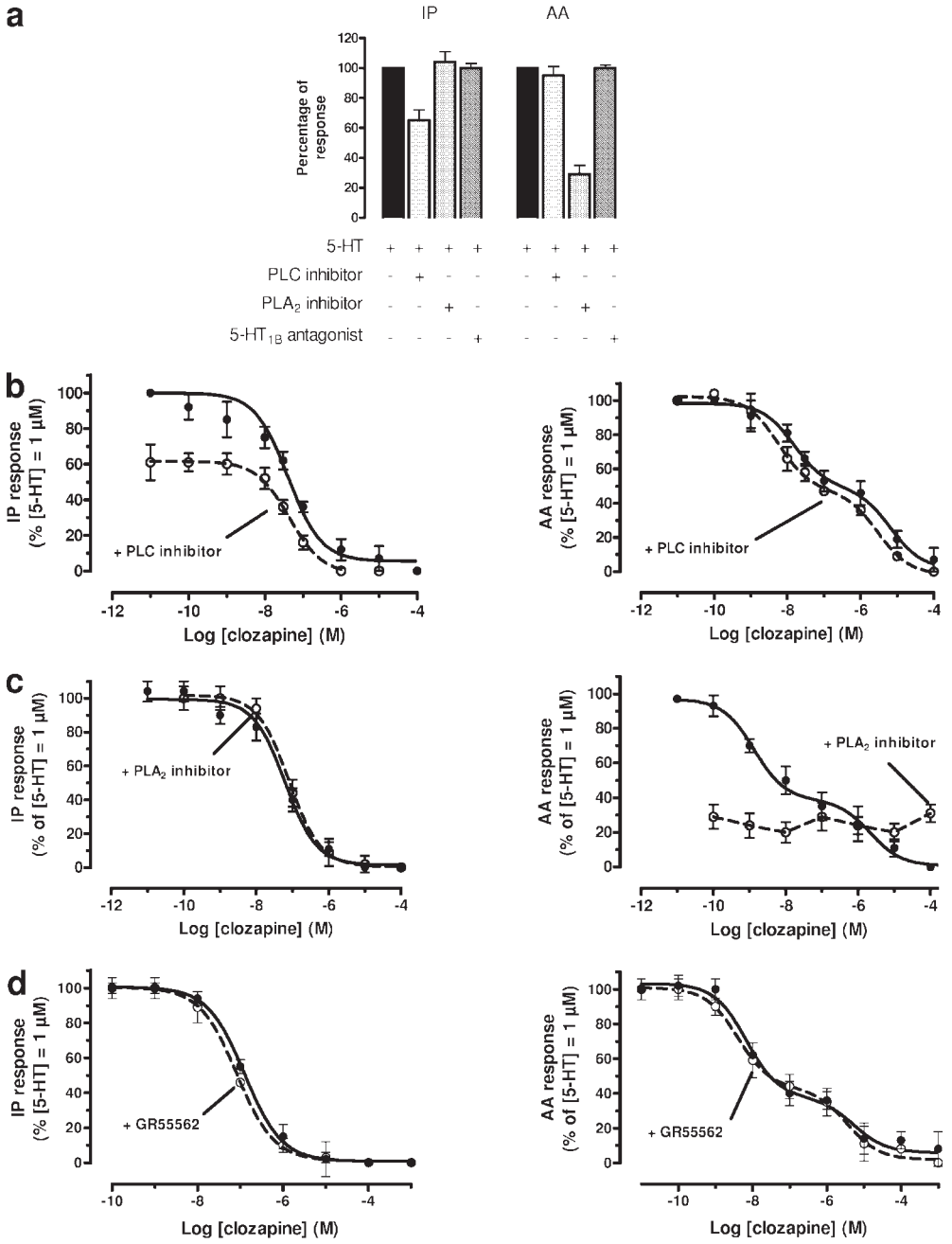

Fig. 4. IP formation and AA release signaling pathways of 5-HT$_{2A}$ receptors are independent of each other and from 5-HT$_{1B}$ endogenous receptors of CHO cells. a, 1 μM 5-HT-induced IP formation (left) and AA release (right) in the absence (black column) and presence of 100 μM PLC inhibitor compound 48/80 (light gray column), 10 μM PLA$_2$ inhibitor aristolochic acid (medium gray column), and 10 μM 5-HT$_{1B}$ antagonist GR55562 (dark gray column). Compound 48/80 reduced 5-HT-induced IP formation by 40%, whereas AA release remained unaltered, aristolochic acid inhibited 5-HT-induced AA release by 80%, and IP formation was unaltered. Neither of the signaling pathways were altered in the presence of the 5-HT$_{1B}$ selective antagonist GR55562. Error bars show S.E.M., n = 3. b, inhibition curves for clozapine on 1 μM 5-HT-elicited IP formation (left) and AA release (right) in the absence (●) and presence (○) of 100 μM PLC inhibitor compound 48/80. It can be observed that partial inhibition of IP formation did not significantly affect clozapine antagonism at the AA pathway ($P > 0.05$, Student's t test). See IC$_{50}$ values listed in Supplementary Table 1. Error bars show S.E.M., n = 3. c, inhibition curves for clozapine on 1 μM 5-HT-elicited IP formation (left) and AA release (right) in the absence (●) and presence (○) of 10 μM PLA$_2$ inhibitor aristolochic acid. It can be observed that inhibition of AA release did not significantly affect clozapine antagonism at the IP pathway ($P > 0.05$, Student's t test). See IC$_{50}$ values listed in Supplementary Table 1. Error bars show S.E.M., n = 3. d, inhibition curves for clozapine on 1 μM 5-HT-elicited IP formation (left) and AA release (right) in the absence (●) and presence (○) of 10 μM 5-HT1B antagonist GR55562. It can be observed that antagonism of this receptor did not significantly affect clozapine antagonism at either of the pathways evaluated. See IC$_{50}$ values listed in Supplementary Table 1. Error bars show S.E.M., n = 3.

tween protomers for some antagonists at the $(R_2)^{**}$ state, must be present. The model leads to the common pharmacological expressions for binding and function by including the proper receptor species (see *Materials and Methods*).

Discussion

GPCR oligomerization has been described both in cultured cells and native tissues (Milligan, 2008). Although there are examples of different GPCRs fully functional as monomers or as oligomers (Meyer et al., 2006; Ernst et al., 2007; Whorton et al., 2007; Milligan, 2008), GPCR oligomerization may constitute a mechanism that facilitates receptor transport, regulates G protein coupling (González-Maeso et al., 2008; Vilardaga et al., 2008), and, as recently shown in heterodimeric receptors, permits direct conformational cross-talk between receptors (González-Maeso et al., 2008; Vilardaga et al., 2008). The possibility that homo-oligomers can also adopt multiple active states extends the capacity of ligands to distinctly modulate different signaling pathways driven by the same receptor. Particularly, antagonist ligands constitute the main source of drugs available, and if they may stabilize particular receptor conformations, it should imply therapeutical consequences. Here we present data supporting the existence of 5-HT_{2A} receptor homodimers in live cells. Our results from coimmunoprecipitation studies are consistent with dimerization/oligomerization of 5-HT_{2A} receptors by noncovalent interactions not resistant to the SDS-PAGE reducing conditions used. In addition, FRET experiments detected a specific FRET signal between 5-$HT_{2A}R^{CFP}$ and 5-$HT_{2A}R^{YFP}$ consistent with the presence of 5-HT_{2A} receptor homodimers in the live cells studied.

5-HT_{2A} receptors are targets of antipsychotics, and it was recently shown that the antipsychotic clozapine but not haloperidol down-regulates the heterodimer mGlu2R-5-HT_{2A} receptor through a 5-HT_{2A}-dependent process (González-Maeso et al., 2008). We report now that these two drugs also differentiate themselves by blocking 5-HT_{2A} responses by two distinct mechanisms. When we studied the binding of different drugs at these receptors, some antagonists, like the atypical antipsychotic drugs clozapine and risperidone, differentiate from others, like the typical antipsychotic drug haloperidol, because they displayed biphasic binding competition curves for agonist [^{3}H](±)DOB-labeled human 5-HT_{2A} receptors, whereas haloperidol displayed monophasic competition curves. These differences were also observed for other 5-HT_{2A} antagonists (ketanserin and MDL100,907 are biphasic inhibitors, whereas mesulergine is a monophasic one).

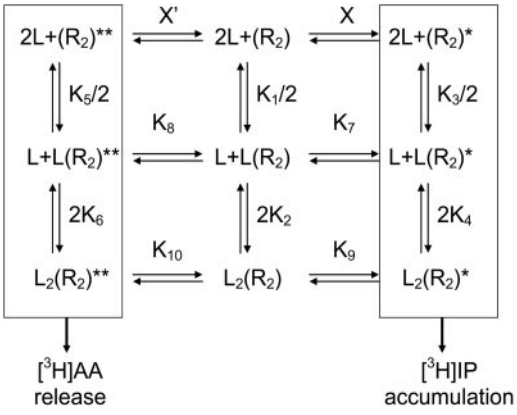

Fig. 5. A three-state dimer receptor model. The model includes one inactive (R_2) and two active [$(R_2)^*$ and $(R_2)^{**}$] receptor states. The $(R_2)^*$ state is proposed to be linked to the IP accumulation pathway, whereas the $(R_2)^{**}$ state is proposed to be linked to the AA release pathway. Although it has been recently suggested that functional receptors may involve asymmetric dimer states (Damian et al., 2006), here, for simplicity, no differences between the protomers of the active states were assumed. Equations are reported in the *Appendix*.

Although the two enantiomers of [^{3}H](±)DOB may have different affinities for 5-HT_{2A} receptors, in a previous study (López-Giménez et al., 2001), we reported saturation studies in which in the presence of Gpp(NH)p, [^{3}H](±)DOB bound to a unique population of receptors in the same cell line as used in the present study. We assumed that if the two enantiomers had different affinities for 5-HT_{2A} receptors in our system, this would have been reflected by two sites in the latter study. Furthermore, a behavior similar to that of [^{3}H](±)DOB in the cell line was observed by autoradiography in brain sections at human native 5-HT_{2A} receptors labeled with [^{125}I](±)DOI, which shows no differences in the affinities of its enantiomers for 5-HT_{2A} receptors (Knight et al., 2004).

Biphasic competition-binding curves can be described by three mechanistic explanations: the presence of different monomeric receptor species, the formation of a receptor-G protein complex in a limited G protein concentration, or the occurrence of receptor dimerization with negative cooperativity between the binding sites of the protomers. In our system, the possible presence of different monomeric receptors had previously been discarded by detailed pharmacological analysis (López-Giménez et al., 2001).

In addition, the absence of Gpp(NH)p effect on the biphasic profile of the binding curves observed for some antagonists indicated that the two phases did not reflect G protein-dependent high- and low-affinity states of the receptor and eliminates the Ternary Complex Model (De Lean A. et al., 1980) and the Extended Ternary Complex Model (Lefkowitz et al., 1993; Samama et al., 1993) as frameworks to interpret the data. Allosteric models (Bosier and Hermans, 2007; Kenakin, 2007b) were also considered inappropriate because complete displacement of radioligands from their specific binding sites was observed for all of the antagonists tested. In this context, negative cooperativity within receptor dimerization seems to be a necessary condition to account for biphasic curves. Indeed, the occurrence of biphasic competition binding curves is currently accepted as indicative of GPCR dimerization, in which binding of a single molecule of agonist to a GPCR dimer will produce negative cooperative effects on the propensity of a second molecule to bind (Chinault et al., 2004; Albizu et al., 2006; Sartania et al., 2007).

A captivating challenge in GPCR homodimerization is to understand its functional consequences in pharmacology, in what extent homodimerization between identical receptors represent the possibility of new pharmacology different from the individual parent *identical* receptors? To gain insight into the functional consequences of the observed antagonist-dependent selective cooperativity at homodimeric 5-HT_{2A} receptors, we first examined the functional behavior on second-messenger signaling pathways of both the atypical antipsychotic clozapine and the typical antipsychotic haloperidol, which showed negative cooperative and noncooperative binding, respectively.

We established an experimental design mimicking that of the binding competition studies and generated concentra-

tion-response curves for both ligands at two noninterlinked 5-HT$_{2A}$-mediated signaling pathways, IP accumulation and AA release. Although haloperidol showed a monophasic inhibition of the 5-HT-dependent activation of both effector pathways, clozapine inhibited the 5-HT-stimulated IP accumulation in a monophasic manner, but intriguingly, its inhibition of the 5-HT-stimulated AA release was biphasic with a strong parallelism with the negative cooperative binding observed for this ligand in radioligand binding assays, even in the fraction of high and low populations and again better described by a dimer receptor model than by a monomer receptor model. We discarded that this behavior could be due to endogenously expressed 5-HT$_{1B}$ receptors or to different kinetics between 5-HT and clozapine in interacting with the receptors. Classic Schild analysis of the concentration-response curves of 5-HT in the presence of clozapine at both effector pathways showed a surmountable and parallel shift of 5-HT concentration-response curve at the IP pathway and a surmountable but noncompetitive antagonism at the AA pathway, indicating that clozapine antagonizes the IP pathway without apparent cooperativity, whereas it shows apparent negative cooperativity at the AA pathway.

We found that all of the other antagonists included in our study showing negative cooperativity in binding assays (ketanserin, risperidone, and MDL100,907) antagonized 5-HT-induced AA release in a biphasic manner differentiating themselves from the monophasic inhibition showed by haloperidol and mesulergine at the same pathway. There was again a strong quantitative correspondence between the negative cooperative binding parameters and the biphasic functional inhibition data obtained at the AA pathway for these ligands. All of the antagonists displayed monophasic inhibition profiles at the IP pathway.

These results therefore provide evidence of a functional antagonist-dependent negative cooperativity in the inhibition of the AA pathway that mirrors the antagonist-dependent negative cooperative binding indicative of 5-HT$_{2A}$ receptor homodimers. To our knowledge, this is the first evidence that antagonists are capable of differently inhibiting signaling pathways at GPCRs.

Although our data are also compatible with a dynamic equilibrium between monomeric and dimeric 5-HT$_{2A}$ receptors showing different functionality (i.e., monomeric receptors signaling through the IP pathway and dimeric receptors signaling through the AA pathway showing the latter ligand-dependent cooperativity), a dimeric form would always be a necessary component of the system, because at least a dimeric form showing cooperativity between the binding sites of the protomers is required for explaining the biphasic antagonism at the AA effector pathway. As described recently (Rovira et al., 2009), the inclusion of monomer species would increase the complexity of the model without providing extra information. Thus, monomer receptor species were not included in the model, and only interconvertible dimeric receptor conformations were considered. To mathematically fit these interconvertible conformations, we propose here a model based on the existence of an equilibrium between the receptor in its inactive dimeric form (R_2) and two distinct active [(R_2)* and (R_2)**] receptor states. This model allows for the differential functional antagonist profiles experimentally observed by assuming a different receptor active conformation for each pathway [e.g., (R_2)* for IP accumulation and (R_2)** for AA release].

We aimed to use this model to account for the specific binding and response curve shapes shown for the different antagonists. Ligand-binding and ligand-response equations can be derived from the proposed model by including the proper receptor species.

A computer simulation using eqs. 12 to 14 from the model depicted in Fig. 5 resulted in profiles that closely match the singular properties found for clozapine in our experiments: namely, monophasic for inhibitory IP response, and biphasic for both binding and inhibitory AA responses (Fig. 6). In brief, the simulation, for a varying concentration of an antagonist B in the presence of a fixed concentration of an agonist A, assumed the following: 1) the agonist displayed null cooperativity at the inactive conformation, (R_2), and positive cooperativity for both the IP and AA pathways; 2) the antagonist displayed null cooperativity for both the inactive conformation and the IP pathway and negative cooperativity for the AA pathway; and 3) the affinity of the antagonist for the second site of the receptor when the first site is occupied by the agonist is greater for the AA pathway conformation than for the IP and inactive conformations. This simulation illustrates the complexity and versatility of a system composed of a dimer receptor with multiple active conformations, in which subtle changes in the ligand-receptor set of interactions may profoundly affect the curve profile.

In summary, both from direct biophysical and indirect binding and functional studies, a dimer arrangement for the 5-HT$_{2A}$ receptor was proposed. The pathway-dependent pharmacological profile shown by some antagonists was explained by a three-state dimer receptor model, including one inactive and two active receptor conformations. The model accounted for the functional selectivity displayed by the antagonist ligands by the cross-talk between protomers through

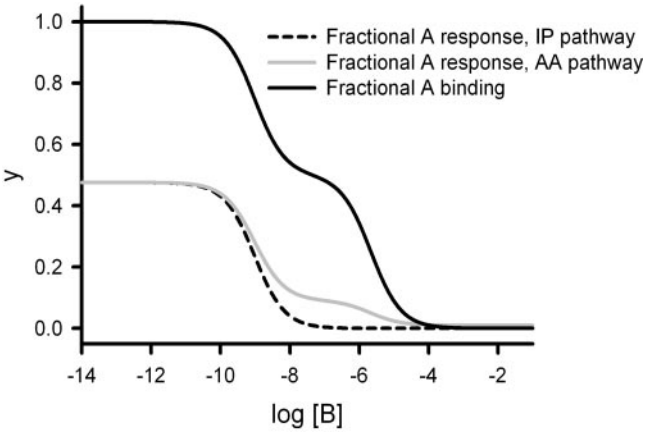

Fig. 6. Simulation of the competitive binding and response inhibition of an antagonist B in the presence of a fixed concentration of an agonist A under the model depicted in Fig. 5. The following values were used in the simulation: [A] = 10^{-1}; X = X′ = 10^{-6}. For the agonist A: $K_1 = K_2 = 10^{-5}$, absence of cooperativity for the inactive conformation; $K_3 = 10^{-5}$, $K_4 = 10^{-12}$, positive cooperativity for the IP pathway; and $K_5 = 10^{-5}$, $K_6 = 10^{-12}$, positive cooperativity for the AA pathway. For the antagonist B: $K_1 = K_2 = 10^{-12}$, absence of cooperativity for the inactive conformation; $K_3 = 10^{-12}$, $K_4 = 10^{-12}$, absence of cooperativity for the IP pathway; and $K_5 = 10^{-16}$, $K_6 = 10^{-12}$, negative cooperativity for the AA pathway. In addition: $K_{11} = K_{12} = 10^{-14}$, and $K_{13} = 10^{-19}$. The affinity of B for the A(R_2)** agonist-receptor complex is greater than for the A(R_2) and A(R_2)* complexes.

the dimer interface. This specific dimer-effector antagonism opens up a new avenue for understanding and reinterpreting the functional meaning of the cooperative binding of many antagonists of GPCRs in general and of 5-HT_{2A} receptors in particular.

Appendix

Equations governing the three-state dimer receptor model (Figure 5):

$$X = \frac{[(R_2)^*]}{[(R_2)]}$$

$$X' = \frac{[(R_2)^{**}]}{[(R_2)]}$$

$$\frac{K_1}{2} = \frac{[(R_2)][L]}{[L(R_2)]}$$

$$2K_2 = \frac{[L(R_2)][L]}{[L_2(R_2)]}$$

$$\frac{K_3}{2} = \frac{[(R_2)^*][L]}{[L(R_2)^*]}$$

$$2K_4 = \frac{[L(R_2)^*][L]}{[L_2(R_2)^*]}$$

$$\frac{K_5}{2} = \frac{[(R_2)^{**}][L]}{[L(R_2)^{**}]}$$

$$2K_6 = \frac{[L(R_2)^{**}][L]}{[L_2(R_2)^{**}]}$$

L stands for a ligand in general. We use the symbol A for the agonist and B for the antagonist. Thus the above model represents the binding of either A or B to the receptor. In addition to "pure" agonist- or antagonist-receptor complexes, we must consider the presence of the mixed species $AB(R_2)$, $AB(R_2)^*$, and $AB(R_2)^{**}$. This can be done by using the following chemical equilibria:

$$B + A(R_2) \xleftrightarrow{K_{11}} AB(R_2), \text{ where } K_{11} = \frac{[B][A(R_2)]}{[AB(R_2)]}$$

$$B + A(R_2)^* \xleftrightarrow{K_{12}} AB(R_2)^*, \text{ where } K_{12} = \frac{[B][A(R_2)^*]}{[AB(R_2)^*]}$$

$$B + A(R_2)^{**} \xleftrightarrow{K_{13}} AB(R_2)^{**}, \text{ where } K_{13} = \frac{[B][A(R_2)^{**}]}{[AB(R_2)^{**}]}$$

Acknowledgments

We thank R. Piña and S. González for excellent technical assistance and J. M. Santamaría for support in the preparation of the manuscript.

References

Albizu L, Balestre MN, Breton C, Pin JP, Manning M, Mouillac B, Barberis C, and Durroux T (2006) Probing the existence of g protein-coupled receptor dimers by positive and negative ligand-dependent cooperative binding. *Mol Pharmacol* **70:** 1783–1791.

Armstrong D and Strange PG (2001) Dopamine D2 receptor dimer formation: evidence from ligand binding. *J Biol Chem* **276:**22621–22629.

Arunlakshana O and Schild HO (1959) Some quantitative uses of drug antagonists. *Br J Pharmacol Chemother* **14:**48–58.

Ayoub MA, Couturier C, Lucas-Meunier E, Angers S, Fossier P, Bouvier M, and Jockers R (2002) Monitoring of ligand-independent dimerization and ligand-induced conformational changes of melatonin receptors in living cells by bioluminescence resonance energy transfer. *J Biol Chem* **277:**21522–21528.

Azzi M, Charest PG, Angers S, Rousseau G, Kohout T, Bouvier M, and Piñeyro G (2003) β-Arrestin-mediated activation of MAPK by inverse agonists reveals distinct active conformations for G protein-coupled receptors. *Proc Natl Acad Sci U S A* **100:**11406–11411.

Baker JG and Hill SJ (2007) Multiple GPCR conformations and signalling pathways: implications for antagonist affinity estimates. *Trends Pharmacol Sci* **28:**374–381.

Bayburt TH, Leitz AJ, Xie G, Oprian DD, and Sligar SG (2007) Transducin activation by nanoscale lipid bilayers containing one and two rhodopsins. *J Biol Chem* **282:**14875–14881.

Berg KA, Harvey JA, Spampinato U, and Clarke WP (2005) Physiological relevance of constitutive activity of 5-HT2A and 5-HT2C receptors. *Trends Pharmacol Sci* **26:**625–630.

Berg KA, Maayani S, Goldfarb J, Scaramellini C, Leff P, and Clarke WP (1998) Effector pathway-dependent relative efficacy at serotonin type 2A and 2C receptors: evidence for agonist-directed trafficking of receptor stimulus. *Mol Pharmacol* **54:**94–104.

Berg KA, Stout BD, Cropper JD, Maayani S, and Clarke WP (1999) Novel actions of inverse agonists on 5-HT2C receptor systems. *Mol Pharmacol* **55:**863–872.

Berridge MJ, Downes CP, and Hanley MR (1982) Lithium amplifies agonist-dependent phosphatidylinositol responses in brain and salivary glands. *Biochem J* **206:**587–595.

Bosier B and Hermans E (2007) Versatility of GPCR recognition by drugs: from biological implications to therapeutic relevance. *Trends Pharmacol Sci* **28:**438–446.

Cheng Y and Prusoff WH (1973) Relationship between the inhibition constant (K1) and the concentration of inhibitor which causes 50 per cent inhibition (I50) of an enzymatic reaction. *Biochem Pharmacol* **22:**3099–3108.

Chidiac P, Green MA, Pawagi AB, and Wells JW (1997) Cardiac muscarinic receptors: cooperativity as the basis for multiple states of affinity. *Biochemistry* **36:** 7361–7379.

Chinault SL, Overton MC, and Blumer KJ (2004) Subunits of a yeast oligomeric G protein-coupled receptor are activated independently by agonist but function in concert to activate G protein heterotrimers. *J Biol Chem* **279:**16091–16100.

Cullen BR (1987) Use of eukaryotic expression technology in the functional analysis of cloned genes. *Methods Enzymol* **152:**684–704.

Damian M, Martin A, Mesnier D, Pin JP, and Banères JL (2006) Asymmetric conformational changes in a GPCR dimer controlled by G-proteins. *EMBO J* **25:**5693–5702.

De Lean A, Stadel JM, and Lefkowitz RJ (1980) A ternary complex model explains the agonist-specific binding properties of the adenylate cyclase-coupled β-adrenergic receptor. *J Biol Chem* **255:**7108–7117.

El-Asmar L, Springael JY, Ballet S, Andrieu EU, Vassart G, and Parmentier M (2005) Evidence for negative binding cooperativity within CCR5-CCR2b heterodimers. *Mol Pharmacol* **67:**460–469.

Elphick GF, Querbes W, Jordan JA, Gee GV, Eash S, Manley K, Dugan A, Stanifer M, Bhatnagar A, Kroeze WK, et al. (2004) The human polyomavirus, JCV, uses serotonin receptors to infect cells. *Science* **306:**1380–1383.

Ernst OP, Gramse V, Kolbe M, Hofmann KP, and Heck M (2007) Monomeric G protein-coupled receptor rhodopsin in solution activates its G protein transducin at the diffusion limit. *Proc Natl Acad Sci U S A* **104:**10859–10864.

Franco R, Casadó V, Mallol J, Ferrada C, Ferré S, Fuxe K, Cortés A, Ciruela F, Lluis C, and Canela EI (2006) The two-state dimer receptor model: a general model for receptor dimers. *Mol Pharmacol* **69:**1905–1912.

Franco R, Casadó V, Mallol J, Ferré S, Fuxe K, Cortés A, Ciruela F, Lluis C, and Canela EI (2005) Dimer-based model for heptaspanning membrane receptors. *Trends Biochem Sci* **30:**360–366.

Giraldo J (2008) On the fitting of binding data when receptor dimerization is suspected. *Br J Pharmacol* **155:**17–23.

Giraldo J, Serra J, Roche D, and Rovira X (2007) Assessing receptor affinity for inverse agonists: Schild and Cheng-Prusoff methods revisited. *Curr Drug Targets* **8:**197–202.

Giraldo J, Vivas NM, Vila E, and Badia A (2002) Assessing the (a)symmetry of concentration-effect curves: empirical versus mechanistic models. *Pharmacol Ther* **95:**21–45.

González-Maeso J, Ang RL, Yuen T, Chan P, Weisstaub NV, López-Giménez JF, Zhou M, Okawa Y, Callado LF, Milligan G, et al. (2008) Identification of a serotonin/glutamate receptor complex implicated in psychosis. *Nature* **452:**93–97.

Herrick-Davis K, Grinde E, Harrigan TJ, and Mazurkiewicz JE (2005) Inhibition of serotonin 5-hydroxytryptamine2c receptor function through heterodimerization: receptor dimers bind two molecules of ligand and one G-protein. *J Biol Chem* **280:**40144–40151.

Herrick-Davis K, Grinde E, and Mazurkiewicz JE (2004) Biochemical and biophysical characterization of serotonin 5-HT2C receptor homodimers on the plasma membrane of living cells. *Biochemistry* **43:**13963–13971.

Herrick-Davis K, Weaver BA, Grinde E, and Mazurkiewicz JE (2006) Serotonin 5-HT2C receptor homodimer biogenesis in the endoplasmic reticulum: real-time visualization with confocal fluorescence resonance energy transfer. *J Biol Chem* **281:**27109–27116.

Hunton DL, Barnes WG, Kim J, Ren XR, Violin JD, Reiter E, Milligan G, Patel DD, and Lefkowitz RJ (2005) β-Arrestin 2-dependent angiotensin II type 1A receptor-mediated pathway of chemotaxis. *Mol Pharmacol* **67:**1229–1236.

Imming P, Sinning C, and Meyer A (2006) Drugs, their targets and the nature and number of drug targets. *Nat Rev Drug Discov* **5:**821–834.

Jarpe MB, Knall C, Mitchell FM, Buhl AM, Duzic E, and Johnson GL (1998) [D-Arg1,D-Phe5,D-Trp7,9,Leu11]Substance P acts as a biased agonist toward neuropeptide and chemokine receptors. *J Biol Chem* **273:**3097–3104.

Kenakin T (1995) Agonist-receptor efficacy. II. Agonist trafficking of receptor signals. *Trends Pharmacol Sci* **16:**232–238.
Kenakin T (2007a) Collateral efficacy in new drug discovery. *Trends Pharmacol Sci* **28:**359–361.
Kenakin T (2007b) Collateral efficacy in drug discovery: taking advantage of the good (allosteric) nature of 7TM receptors. *Trends Pharmacol Sci* **28:**407–415.
Kent RS, De Lean A, and Lefkowitz RJ (1980) A quantitative analysis of beta-adrenergic receptor interactions: resolution of high and low affinity states of the receptor by computer modeling of ligand binding data. *Mol Pharmacol* **17:**14–23.
Knight AR, Misra A, Quirk K, Benwell K, Revell D, Kennett G, and Bickerdike M (2004) Pharmacological characterisation of the agonist radioligand binding site of 5-HT$_{2A}$, 5-HT$_{2B}$ and 5-HT$_{2C}$ receptors. *Naunyn Schmiedebergs Arch Pharmacol* **370:**114–123.
Leff P (1995) The two-state model of receptor activation. *Trends Pharmacol Sci* **16:**89–97.
Leff P, Scaramellini C, Law C, and McKechnie K (1997) A three-state receptor model of agonist action. *Trends Pharmacol Sci* **18:**355–362.
Lefkowitz RJ, Cotecchia S, Samama P, and Costa T (1993) Constitutive activity of receptors coupled to guanine nucleotide regulatory proteins. *Trends Pharmacol Sci* **14:**303–307.
López-Giménez JF, Villazón M, Brea J, Loza MI, Palacios JM, Mengod G, and Vilaró MT (2001) Multiple conformations of native and recombinant human 5-hydroxytryptamine$_{2a}$ receptors are labeled by agonists and discriminated by antagonists. *Mol Pharmacol* **60:**690–699.
Mercier JF, Salahpour A, Angers S, Breit A, and Bouvier M (2002) Quantitative assessment of β1- and β2-adrenergic receptor homo- and heterodimerization by bioluminescence resonance energy transfer. *J Biol Chem* **277:**44925–44931.
Meyer BH, Segura JM, Martinez KL, Hovius R, George N, Johnsson K, and Vogel H (2006) FRET imaging reveals that functional neurokinin-1 receptors are monomeric and reside in membrane microdomains of live cells. *Proc Natl Acad Sci U S A* **103:**2138–2143.
Milligan G (2004) G protein-coupled receptor dimerization: function and ligand pharmacology. *Mol Pharmacol* **66:**1–7.
Milligan G (2008) A day in the life of a G protein-coupled receptor: the contribution to function of G protein-coupled receptor dimerization. *Br J Pharmacol* **153 (Suppl 1):**S216–S229.
Rovira X, Vivó M, Serra J, Roche D, Strange PG, and Giraldo J (2009) Modelling the interdependence between the stoichiometry of receptor oligomerization and ligand binding for a coexisting dimer/tetramer receptor system. *Br J Pharmacol* **156:**28–35.
Samama P, Cotecchia S, Costa T, and Lefkowitz RJ (1993) A mutation-induced activated state of the β2-adrenergic receptor. Extending the ternary complex model. *J Biol Chem* **268:**4625–4636.
Sartania N, Appelbe S, Pediani JD, and Milligan G (2007) Agonist occupancy of a single monomeric element is sufficient to cause internalization of the dimeric beta2-adrenoceptor. *Cell Signal* **19:**1928–1938.
Scaramellini C and Leff P (2002) Theoretical implications of receptor coupling to multiple G proteins based on analysis of a three-state model. *Methods Enzymol* **343:**17–29.
Urban JD, Clarke WP, von Zastrow M, Nichols DE, Kobilka B, Weinstein H, Javitch JA, Roth BL, Christopoulos A, Sexton PM, et al. (2007) Functional selectivity and classical concepts of quantitative pharmacology. *J Pharmacol Exp Ther* **320:**1–13.
Urizar E, Montanelli L, Loy T, Bonomi M, Swillens S, Gales C, Bouvier M, Smits G, Vassart G, and Costagliola S (2005) Glycoprotein hormone receptors: link between receptor homodimerization and negative cooperativity. *EMBO J* **24:**1954–1964.
Vilardaga JP, Bünemann M, Krasel C, Castro M, and Lohse MJ (2003) Measurement of the millisecond activation switch of G protein-coupled receptors in living cells. *Nat Biotechnol* **21:**807–812.
Vilardaga JP, Nikolaev VO, Lorenz K, Ferrandon S, Zhuang Z, and Lohse MJ (2008) Conformational cross-talk between alpha2A-adrenergic and mu-opioid receptors controls cell signaling. *Nat Chem Biol* **4:**126–131.
Vilardaga JP, Steinmeyer R, Harms GS, and Lohse MJ (2005) Molecular basis of inverse agonism in a G protein-coupled receptor. *Nat Chem Biol* **1:**25–28.
Weiss J, Morgan P, Lutz M, and Kenakin T (1996) The cubic ternary complex receptor-occupancy model I. Model description. *J Theor Biol* **178:**151–167.
Whorton MR, Bokoch MP, Rasmussen SG, Huang B, Zare RN, Kobilka B, and Sunahara RK (2007) A monomeric G protein-coupled receptor isolated in a high-density lipoprotein particle efficiently activates its G protein. *Proc Natl Acad Sci U S A* **104:**7682–7687.
Wisler JW, DeWire SM, Whalen EJ, Violin JD, Drake MT, Ahn S, Shenoy SK, and Lefkowitz RJ (2007) A unique mechanism of β-blocker action: carvedilol stimulates β-arrestin signaling. *Proc Natl Acad Sci U S A* **104:**16657–16662.
Wreggett KA and Wells JW (1995) Cooperativity manifest in the binding properties of purified cardiac muscarinic receptors. *J Biol Chem* **270:**22488–22499.
Wu C, Yoder EJ, Shih J, Chen K, Dias P, Shi L, Ji XD, Wei J, Conner JM, Kumar S, et al. (1998) Development and characterization of monoclonal antibodies specific to the serotonin 5-HT2A receptor. *J Histochem Cytochem* **46:**811–824.
Zacharias DA, Violin JD, Newton AC, and Tsien RY (2002) Partitioning of lipid-modified monomeric GFPs into membrane microdomains of live cells. *Science* **296:**913–916.

Address correspondence to: Dr. María Isabel Loza, Dpto. Farmacología, Facultad de Farmacia, Campus Sur. 15782 Santiago de Compostela, Spain. E-mail: mabel.loza@usc.es